FUDMA Journal of Sciences (FJS)
ISSN online: 2616-1370
ISSN print: 2645 - 2944
Vol. 9 No. 8, August, 2025, pp 198 – 209
DOI: https://doi.org/10.33003/fjs-2025-0908-3796

HEAT AND MASS TRANSFER FLOW THROUGH POROUS MEDIUM WITH VARIABLE THERMAL CONDUCTIVITY AND SUCTION EFFECTS

***[1]Abubakar Sadiq Uba, [1]Emem Ayankop Andi, [2]Abubakar Abdullahi Wachin and [3]Joseph Kpop Moses**

[1]Department of Mathematical Sciences, Nigerian Defense Academy, Kaduna, Nigeria
[2]Department of Mathematics, AFIT, Kaduna, Nigeria
[3]Department of Mathematical Sciences, Kaduna State University, Kaduna, Nigeria

*Corresponding authors' email: uba.abubakar@gmail.com

ABSTRACT

This study investigates heat and mass transfer flow through a porous medium with variable thermal conductivity and suction effects. Unsteady natural convection with magnetic field, radiation and pressure gradient were considered. Perturbation method was employed to derive analytical expressions for the dimensionless velocity, temperature, and concentration profiles. The influence of key dimensionless parameters—including variable thermal conductivity(λ), temperature and mass buoyancy parameters (R, R_C), magnetic field strength(M), suction parameter(S), Darcy number (D_a), mass Grashof numbers (G_C), radiation parameter (N), Prandtl number (P_r), chemical reaction rate (K_r), Schmidt number (S_C), and pressure gradient (Ω)—were analyzed in detail. Results showed: increased in (λ), (R, R_C), (D_a), (G_C), and (N) enhanced velocity while (M), (S), (S_C) and (Ω)suppressed it. Temperature rises with increased (λ), (R) and (N) but decreased with (S) and (P_r). Species concentration decreased with stronger (S), (S_C) and (K_r). Additionally, Skin friction (C_f), Nusselt number (N_u) and Sherwood number (S_h) exhibited significant sensitivity to variations in the governing parameters. The findings provided valuable insight into flow behavior in porous media with applications in geophysics, chemical engineering, and energy systems.

Keywords: Heat and Mass Transfer, Porous Medium, Variable Thermal Conductivity, Suction

INTRODUCTION

The study of heat and mass transfer flow through porous media is vital in various industrial applications such as heat exchangers, chemical reactors and fuel cells (Bejan, 2013; Incropera & Demitt, 2018). The presence of porous medium in the channel significantly alter flow behavior, heat transfer, and mass transport processes (Ingham & Pop, 2017). In recent years, there has been growing interest in studying the effect of variable thermal conductivity or suction on heat or mass transfer flow in porous media (Abdollahi & Mahmuodi, 2020; Rashidi & Esfahani, 2020; Singh & Kumar, 2020). In a recent literature survey, Kaviany (2012) investigated heat transfer in porous media. It was observed that mechanisms such as conduction, convection, and radiation influence heat transfer process in porous media. Kuznetsov and Nield (2013) investigated the effect of variable thermal conductivity on heat transfer in a channel filled with porous medium. Temperature distribution and Nusselt number were analyzed in the channel flow configuration, analytical and numerical solutions were presented. Results indicated that an increase in thermal conductivity leads to a more efficient heat transfer process, while a decrease in thermal conductivity reduces the rate of heat transfer. Porous medium also enhances heat transfer by promoting convection. Mahmoudi *et al*. (2017) studied mass transfer in a channel filled with porous medium, focusing on the effects of variable thermal conductivity. Singh *et al*. (2019) focused on the numerical study of heat transfer in a channel filled with a porous medium, emphasizing the effects of suction.

The impact of suction on the convective heat transfer process in a porous medium was examined, using computational fluid dynamics (CFD) simulations to model the flow and heat transfer characteristics. The study found that suction enhances heat transfer by increasing the fluid velocity near the surface and improving the convective heat transfer coefficient. Singh and Kumar (2020) focused on the combined effects of variable thermal conductivity and suction on heat transfer in a porous channel. Their findings suggest that optimizing suction rates and considering the variations in thermal conductivity could improve the heat transfer efficiency in various industrial applications, including cooling and heating systems in porous materials. Kaita *et al*. (2024) studied heat and mass transfer in a channel filled with porous medium in the presence variable thermal conductivity considering chemical reaction, porosity and buoyancy distribution force. Dimensionless governing equations were solved analytically using perturbation technique. Analytical solutions obtained are presented in graphs for the fluid flow on heat and mass transfer characteristics for different values of parameters involved in the problem, it was observed that velocity increases with increasing Grashof number, mass Buoyancy and magnetic field parameter while reverse is the case with increase porosity parameter. To the best of our knowledge the problem of heat and mass transfer flow in a channel filled with porous medium in the presence of variable thermal conductivity and suction effects has not been studied. In this work, we study the combined effects of variable thermal conductivity and suction on Heat and mass transfer flow through porous medium. We discussed the effect of the parameters involved on the flow; compute the skin frictions, rate of heat transfer and the rate of mass transfer at the walls.

MATERIALS AND METHODS

Mathematical Formulation

The unsteady, natural convection, heat and mass transfer flow of an electrically, conducting incompressible viscous fluid, having temperature dependent thermal conductivity between two vertical walls under the influence of a uniform transverse magnetic field of strength B_0 as shown in Figure 1 below is chosen. It is assumed that both the fluid and the walls are at rest and maintained a constant temperature T_m^* and the mass concentration C_m^*. At time $t^* > 0$, the wall is maintained at uniform temperature T_h^* and uniform concentration C_h^* which are higher than T_c^* and C_c^* respectively. A Cartesian coordinate system with x^* axis along the upward direction and the y^* axis normal to it is chosen. Note, superscript (*) represents parameters with dimension.

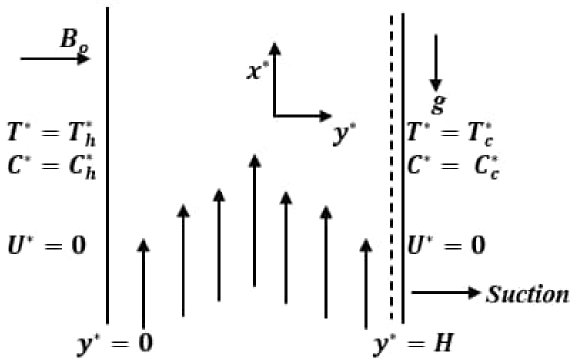

Figure 1: Physical Configuration of the Flow System

Thermal conductivity (K_f) which obeys linear temperature law according to $K_f = k_m\ [1 + \delta(T^*] - T_m^*)]$, where km is the fluid free thermal conductivity and δ is a constant dependent on the fluid ($\delta > 0$ for lubrication oils, hydromagnetic working fluids and $\delta > 0$ for air or water). Under these assumptions, along with Boussinesq's approximation, the governing equations for continuity, momentum, energy, and concentration in laminar incompressible boundary layer flow can be written as follow:

$$\frac{\partial S^*}{\partial y^*} = 0 \quad \rightarrow \quad S^* = -S_0 \tag{1}$$

$$\frac{\partial U^*}{\partial t^*} + S^*\frac{\partial U^*}{\partial y^*} = -\frac{1}{\rho}\frac{\partial p^*}{\partial x^*} + \nu\frac{\partial^2 U^*}{\partial y^{*2}} + g\beta^*(C^* - C_m^*) + g\beta(T^* - T_m^*) - \sigma\frac{\beta_0^2 u^*}{\rho} - \frac{1}{K}U^* \tag{2}$$

$$\frac{\partial T^*}{\partial t^*} + S^*\frac{\partial U^*}{\partial y^*} = \frac{1}{\rho C_p}\frac{\partial}{\partial y}\left(K_f\frac{\partial T^*}{\partial y^*}\right) - \frac{\partial q_r}{\partial y^*} \tag{3}$$

$$\frac{\partial C^*}{\partial t^*} + S^*\frac{\partial C^*}{\partial y^*} = D\frac{\partial^2 C^*}{\partial y^{*2}} - K^*(C^* - C_m^*) \tag{4}$$

The corresponding initial and boundary conditions are prescribed as follows:

$$\left.\begin{aligned} &t^* \le 0;\ U^* = 0, T^* = T_m^*, C^* = C_m^*, \quad for\ 0 \le y^* \le H \\ &t^* > 0;\ U^* = 0, T^* = T_h^*, C^* = C_h^*, at\ y^* = 0 \\ &U^* = 0, T^* = T_c^*, C^* = C_c^*, at\ y^* = H \end{aligned}\right\} \tag{5}$$

where ν, σ, ρ are kinematic viscosity, conductivity of the fluid and density respectively, g, β, β^* are gravitational force, coefficient of the thermal expansion and concentration expansion coefficient respectively, D, B_0, C_P are chemical molecular diffusivity, electromagnetic induction and specific heat at constant pressure respectively, $t^*, T^*, C^*$are time, fluid temperature and concentration respectively, $U^* and\ S^*$ are velocity components in $x\ and\ y$ directions respectively, $k^* and\ Da$ are chemical reaction rate and porosity. T_m^*, T_h^*, T_c^* are initial temperature of the fluid, temperature of the wall at $y^*= 0$, temperature of the wall at y^* = H respectively, C_m^*, C_h^*, C_c^* are initial concentration of the fluid, concentration of the wall at $y^* = 0$, concentration of the wall at $y^* = H$ respectively.

The non-dimensional quantities introduced in the above equations are as follows:

$$U = \frac{U^*\nu}{g\beta(T_h^* - T_m^*)H^2}, \quad Y = \frac{y^*}{H}, \quad R_C = \frac{(C_c^* - C_m^*)}{(C_h^* - C_m^*)},$$

$$D_a = \frac{K\nu}{H^2}, \quad M^2 = \sigma\frac{\beta_0{}^2H^2}{\nu\rho},$$

$$N = \frac{4\alpha^2H^2(T_h^* - T_m^*)}{\nu}, \quad t = \frac{t^*}{H^2}, \quad \theta = \frac{(T^* - T_m^*)}{(T_h^* - T_m^*)},$$

$$P_r = \frac{\nu\rho C_p}{K_m}, \quad \lambda = \delta(T_h^* - T_m^*),$$

$$G_C = \frac{g\beta^*(C^* - C_m^*)}{g\beta(T_h^* - T_m^*)}, \quad S_C = \frac{\nu}{D}, \quad C = \frac{(C^* - C_m^*)}{(C_h^* - C_m^*)},$$

$$K_r = \frac{H^2K^*}{\nu},$$

$$\frac{\partial q_r}{\partial y^*} = 4(T_m^* - T^*),\ S = -\frac{S^*H}{\nu},\ R = \frac{(T_c^* - T_m^*)}{(T_h^* - T_m^*)},\ \frac{1}{Da} = \frac{H^2}{K\nu} \tag{6}$$

Applying (6) to (2), (3), (4), (5), the following governing equations in non-dimensional form are obtained:

$$\frac{\partial U}{\partial t} - s\frac{\partial U}{\partial y} = \Omega + \frac{\partial^2 U}{\partial y^2} + \theta + GcC - \left(M^2 + \frac{1}{Da}\right)U \tag{7}$$

$$\frac{\partial \theta}{\partial t} - s\frac{\partial \theta}{\partial y} = \frac{1}{P_r}\left[\left(\frac{\partial \theta}{\partial y}\right)^2 + (1 + \lambda\theta)\frac{\partial^2 \theta}{\partial y^2}\right] + N\theta \tag{8}$$

$$\frac{\partial C}{\partial t} - s\frac{\partial C}{\partial y} = \frac{1}{Sc}\frac{\partial^2 C}{\partial y^2} - K_rC \tag{9}$$

Where $\Omega = -\frac{1}{\rho g\beta(T_h^* - T_m^*)}\frac{\partial p^*}{\partial x^*}$

With the following initial and boundary conditions in dimensionless form:

$$\left.\begin{aligned} &t \le 0;\ U = 0, \quad \theta = 0, \quad C = 0, \quad for\ all\ y \\ &t > 0;\ U = 0, \quad \theta = 1, \quad C = 1, \quad at\ y = 0 \\ &U = 0, \quad \theta = R, \quad C = Rc, \quad at\ y = 1 \end{aligned}\right\} \tag{10}$$

Where S is suction, λ is the variable thermal conductivity, Ω is the pressure gradient, N is the radiation parameter, Da is the porosity parameter, G_c is the Solutal Grashof number, M is the Magnetic field parameter, P_r is the Prandtl number, S_c is the Schmidt number, R_c is the mass buoyancy parameter, R is the temperature buoyancy parameter and K_r is the chemical reaction parameter.

Method of Solution

To solve equation (7), (8) and (9) subject to the boundary condition (10) the functions $U(y,t)$, $\theta(y,t)$ and $C(y,t)$ were expanded in the perturbative parameter λ. We assume $\lambda \ll 1$ while ignoring higher powers of λ as their impact is minimal in leading order.

$$U(y,t) = U_0(y) + \lambda U_1(y)e^{i\omega t} \tag{11}$$

$$\theta(y,t) = \theta_0(y) + \lambda\theta_1(y)e^{i\omega t} \tag{12}$$

$$C(y,t) = C_0(y) + \lambda C_1(y)e^{i\omega t} \tag{13}$$

The first terms in each equation (11), (12) and (13) are called the harmonic terms while the second terms are called the non-harmonic terms. Now, substituting equation (11), (12) and (13) into equation (7), (8) and (9) and equating the coefficients of the harmonic and non-harmonic terms:

$$\frac{\partial^2 U_0}{\partial y^2} + S\frac{\partial U_0}{\partial y} - L_3 U_0 = -\Omega - \theta_0 - G_c C_0 \quad (14)$$

$$\frac{\partial^2 U_1}{\partial y^2} + S\frac{\partial U_1}{\partial y} - L_4 U_1 = -\Omega - \theta_1 - G_c C_1 \quad (15)$$

$$\frac{\partial^2 \theta_0}{\partial y^2} + SP_r\frac{\partial \theta_0}{\partial y} + NP_r\theta_0 = 0 \quad (16)$$

$$\frac{\partial^2 \theta_1}{\partial y^2} + SP_r\frac{\partial \theta_1}{\partial y} + L_2\theta_1 = 0 \quad (17)$$

$$\frac{\partial^2 C_0}{\partial y^2} + SS_C\frac{\partial C_0}{\partial y} - K_r S_C C_0(y) = 0 \quad (18)$$

$$\frac{\partial^2 C_1}{\partial y^2} + SS_C\frac{\partial C_1}{\partial y} - L_1 C_1(y) = 0 \quad (19)$$

Where: $L_1 = S_C(K_r + \omega)$, $L_2 = P_r(N - i\omega)$, $L_3 = \left(M^2 + \frac{1}{Da}\right)$ and $L_4 = (L_3 - i\omega)$

The corresponding relevant boundary condition becomes:

$$\left.\begin{matrix} t \le 0;\ U_0 = 0,\ \theta_0 = 1, C_0 = 0, & for\ all\ y \\ t > 0;\ U_1 = 0,\ \theta_1 = R, C_1 = 1, & at\ y = 0 \end{matrix}\right\} \quad (20)$$

Solving (14) to (19) with (20) the solution of the governing equations is obtained as:

$$U(y,t) = (A_9 e^{m_9 y} + A_{10}e^{m_{10}y} + K_0 + K_1 e^{m_1 y} + K_2 e^{m_2 y} + K_3 e^{m_5 y} + K_4 e^{m_6 y}) + \lambda(A_{11}e^{m_{11}y} + A_{12}e^{m_{12}y} + K_5 e^{m_3 y} + K_6 e^{m_4 y} + K_7 e^{m_7 y} + K_8 e^{m_8 y} + K_9)e^{i\omega t} \quad (21)$$

$$\theta(y,t) = (A_5 e^{m_5 y} + A_6 e^{m_6 y}) + \lambda(A_7 e^{m_7 y} + A_8 e^{m_8 y})e^{i\omega t} \quad (22)$$

$$C(y,t) = (A_1 e^{m_1 y} + A_2 e^{m_2 y}) + \lambda(A_3 e^{m_3 y} + A_4 e^{m_4 y})e^{i\omega t} \quad (23)$$

The Skin Friction C_f: shear stress at the walls:

$$C_{f_0} = \left.\frac{\partial U}{\partial y}\right|_{y=0} = (A_9 m_9 + A_{10}m_{10} + K_1 m_1 + K_2 m_2 + K_3 m_5 + K_4 m_6) + \lambda(A_{11}m_{11} + A_{12}m_{12} + K_5 m_3 + K_6 m_4 + K_7 m_7 + K_8 m_8 + K_9)e^{i\omega t} \quad (24)$$

$$C_{f_1} = \left.\frac{\partial U}{\partial y}\right|_{y=1} = (A_9 e^{m_9} + A_{10}e^{m_{10}} + K_0 + K_1 e^{m_1} + K_2 e^{m_2} + K_3 e^{m_5} + K_4 e^{m_6}) + \lambda(A_{11}e^{m_{11}} + A_{12}e^{m_{12}} + K_5 e^{m_3} + K_6 e^{m_4} + K_7 e^{m_7} + K_8 e^{m_8} + K_9)e^{i\omega t} \quad (25)$$

The Nusselt number N_u: rate of heat transfer at the walls:

$$N_{f_0} = \left.\frac{\partial \theta}{\partial y}\right|_{y=0} = (A_5 m_5 + A_6 m_6) + \lambda(A_7 m_7 + A_8 m_8)e^{i\omega t} \quad (26)$$

$$N_{f_1} = \left.\frac{\partial \theta}{\partial y}\right|_{y=1} = (A_5 m_5 e^{m_5} + A_6 m_6 e^{m_6}) + \lambda(A_7 m_7 e^{m_7} + A_8 m_8 e^{m_8})e^{i\omega t} \quad (27)$$

The Sherwood number S_u: rate of mass transfer at the walls:

$$S_{f_0} = \left.\frac{\partial C}{\partial y}\right|_{y=0} = (A_1 m_1 + A_2 m_2) + \lambda(A_3 m_3 + A_4 m_4)e^{i\omega t} \quad (28)$$

$$S_{f_1} = \left.\frac{\partial C}{\partial y}\right|_{y=1} = (A_1 m_1 e^{m_1} + A_2 m_2 e^{m_2}) + \lambda(A_3 m_3 e^{m_4} + A_4 m_4 e^{m_4})e^{i\omega t} \quad (29)$$

Where $A_1\ to A_{12}$, $m_1\ to m_{12}$, $L_1\ to L_8$ and K_0 , $K_1\ to K_9$ are constants.

RESULTS AND DISCUSSION

For computation of analytical expression of the velocity, temperature and concentration were taken using graphs obtained from MATLAB. The values of the pertinent parameters are: $M = 1$, $N = 1$, $t = 1, \pi = 180°, m = 0.5, A = 0.3$, $\omega = 1.0$, $\lambda = 0.002$

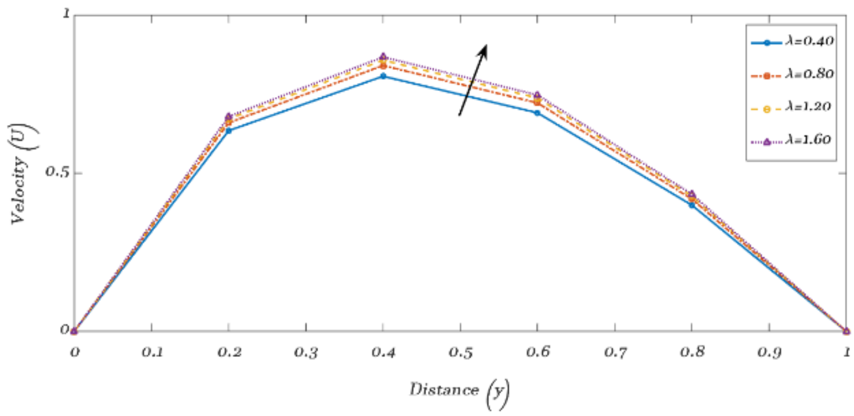

Figure 2: Effect of Variable Thermal Conductivity λ on Velocity Profile

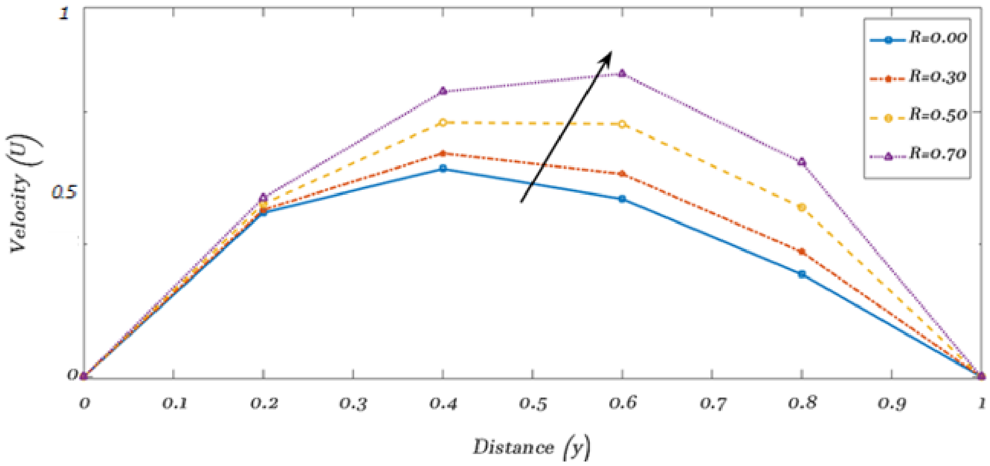

Figure 3: Effect of Temperature Buoyancy parameter R on Velocity Profile

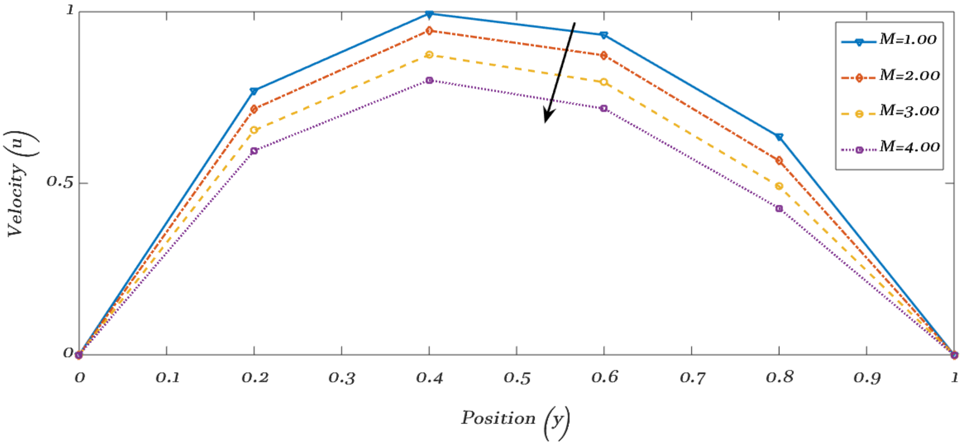

Figure 4: Effect of Magnetic Parameter M on Velocity Profile

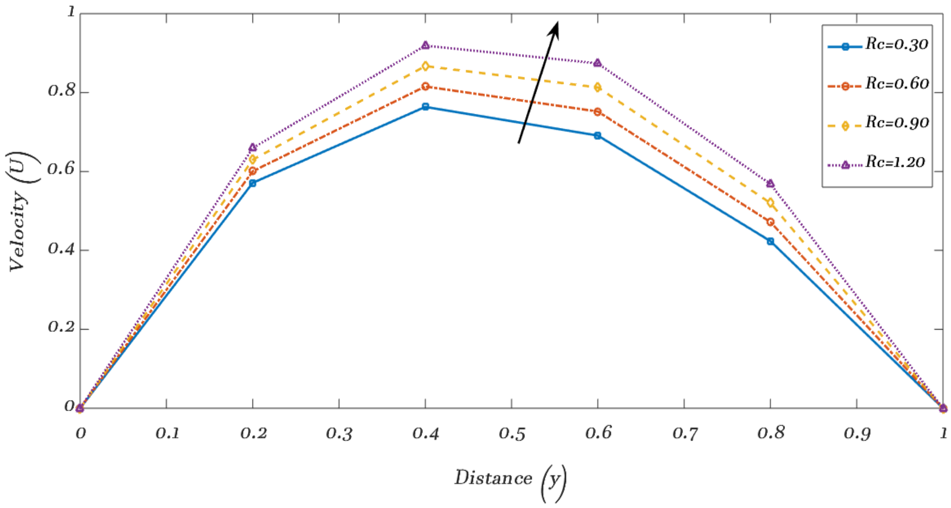

Figure 5: Effect of Mass Buoyancy Parameter Rc on Velocity Profile

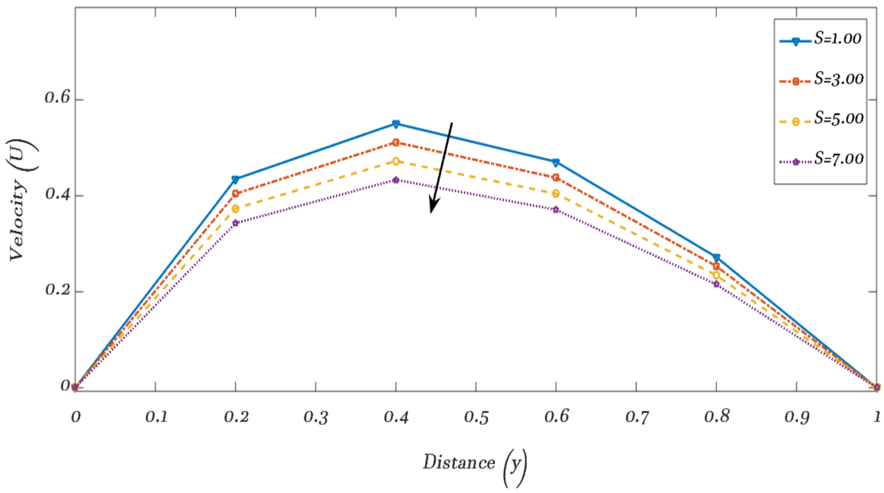

Figure 6: Effect of Suction parameter S on Velocity Profile

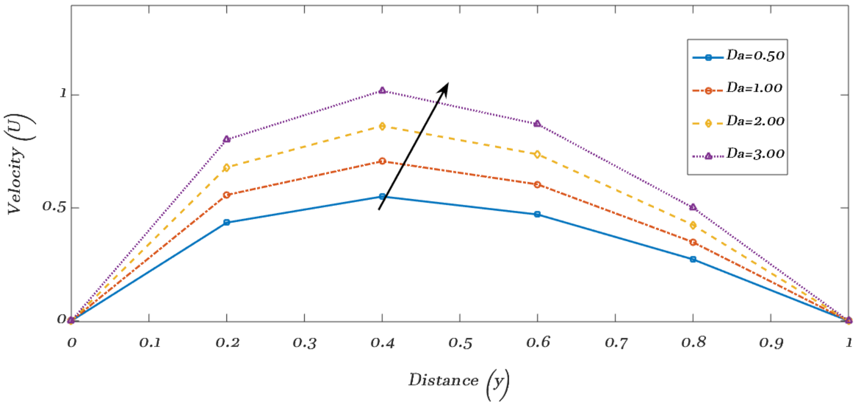

Figure 7: Effect of Darcy parameter D_a on Velocity Profile

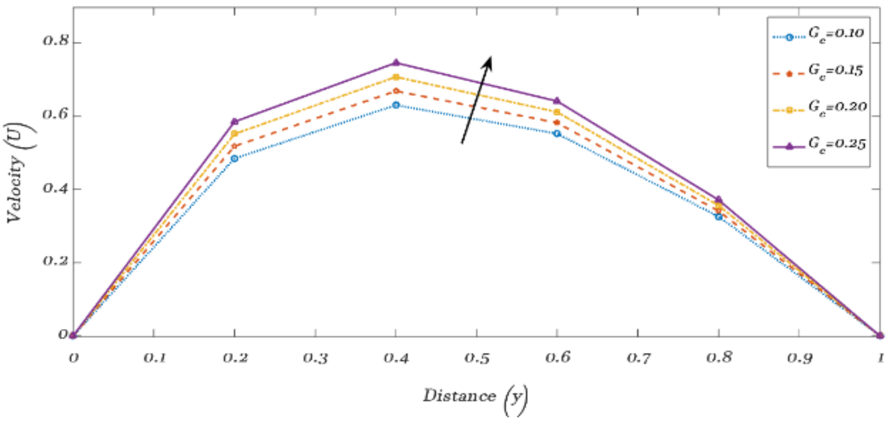

Figure 8: Effect of Grashof number due to mass transfer G_c on Velocity Profile

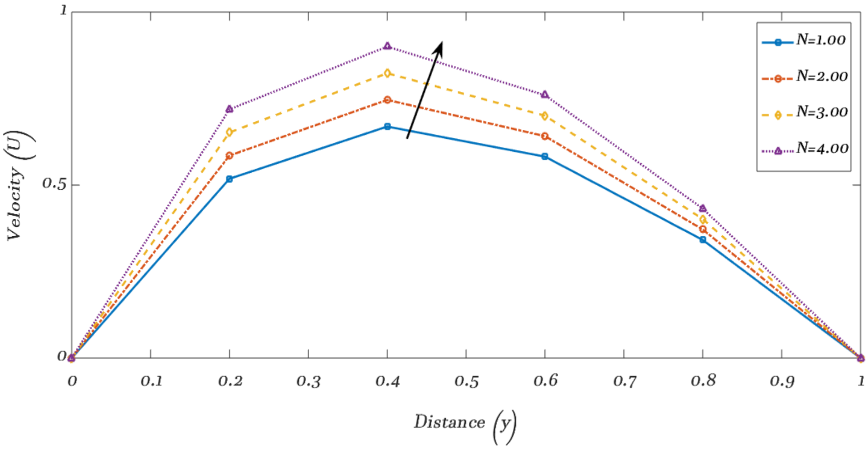

Figure 9: Effect of Radiation parameter N on Velocity Profile

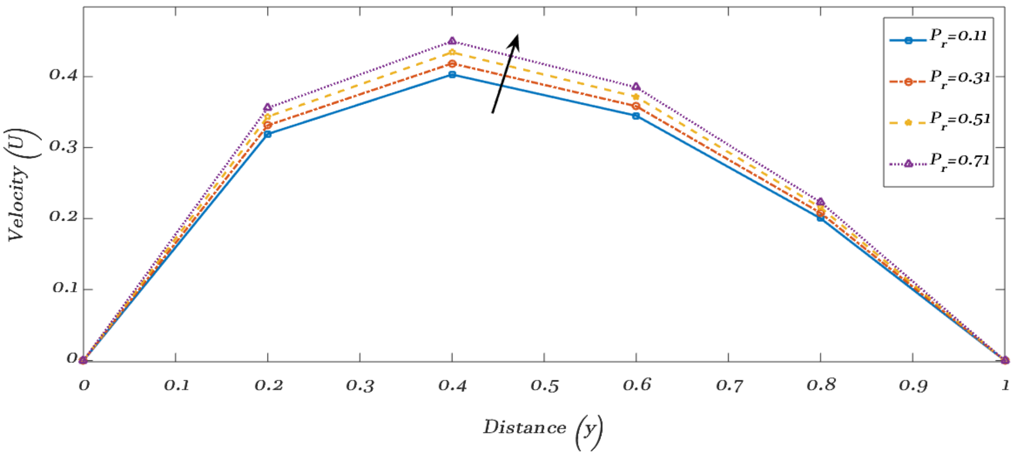

Figure 10: Effect of Prandtl number P_r on Velocity Profile

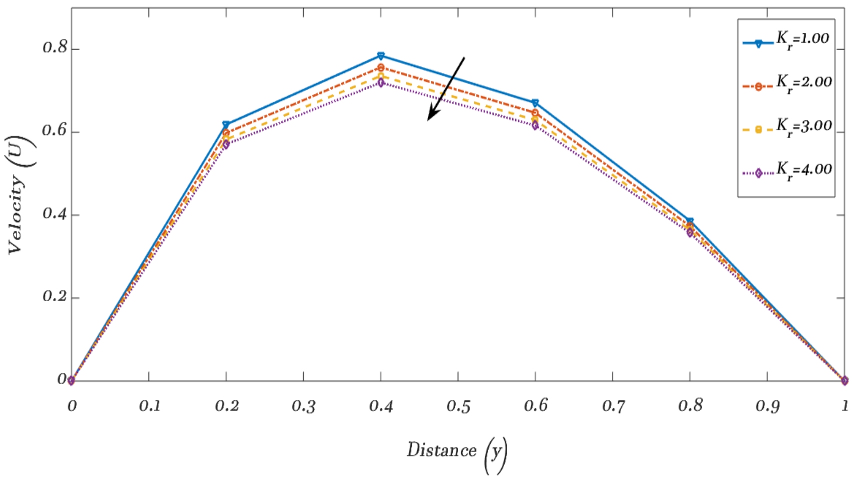

Figure 11: Effect of Chemical Reaction parameter K_r on Velocity Profile

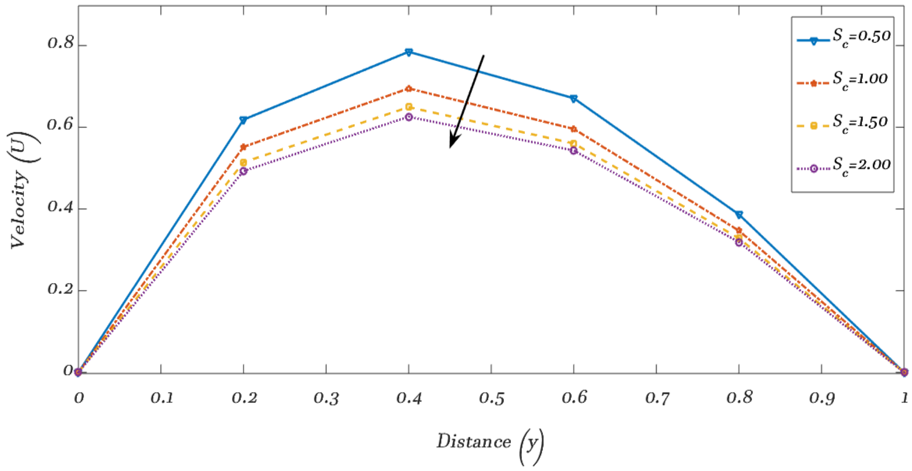

Figure 12: Effect of Schmidt number S_c on Velocity Profile

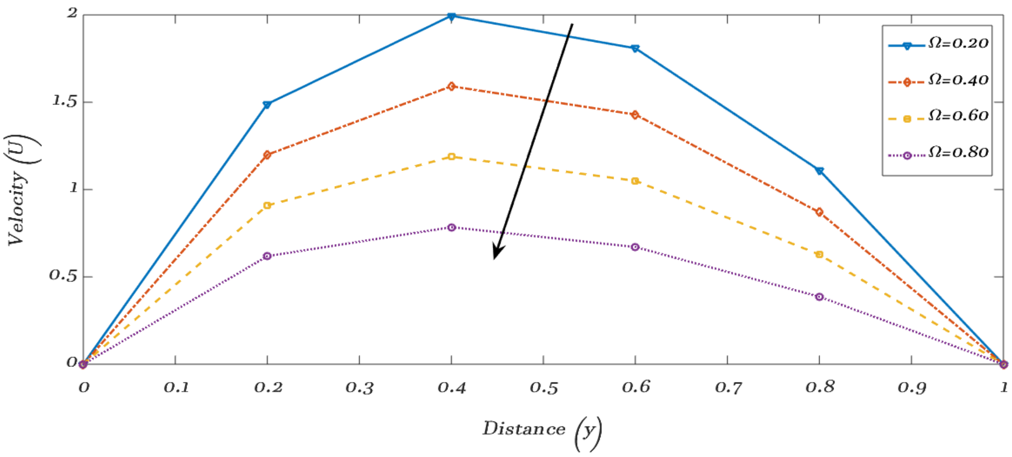

Figure 13: Effect of Pressure Gradient Ω on Velocity Profile

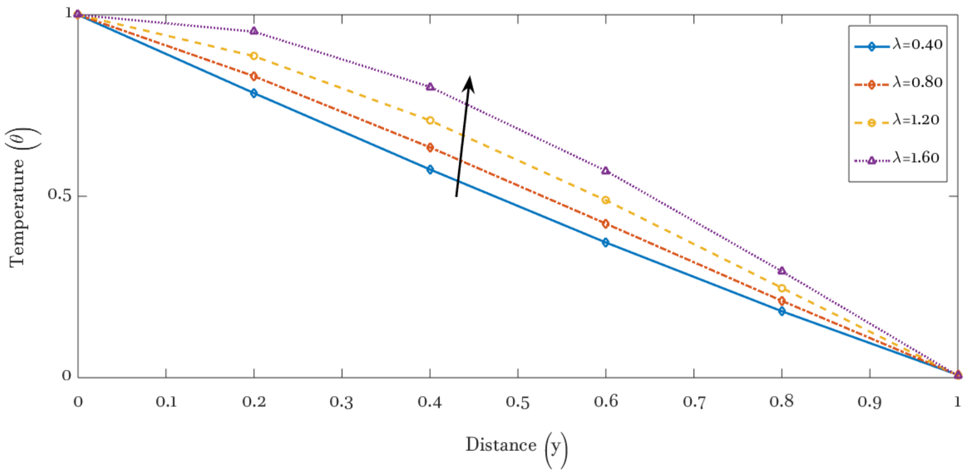

Figure 14: Effect of Variable Thermal Conductivity λ on Temperature Profile

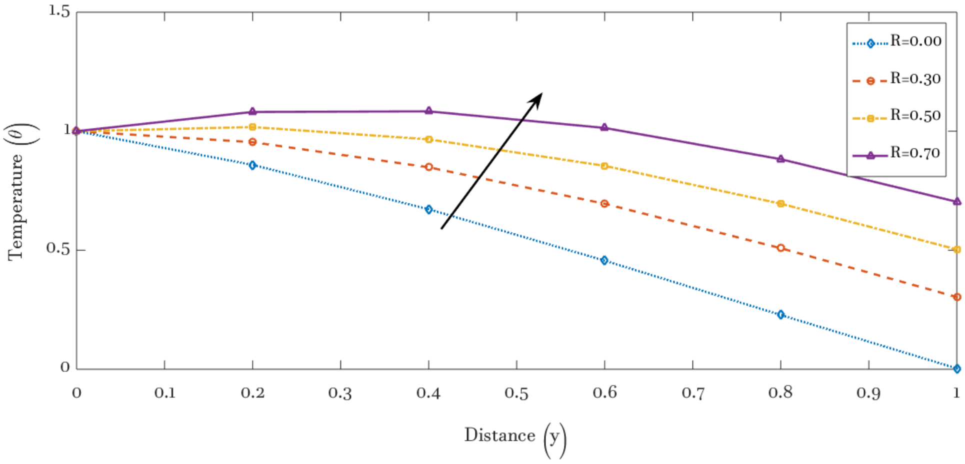

Figure 15: Effect of Temperature Buoyancy Parameter R on Temperature Profile

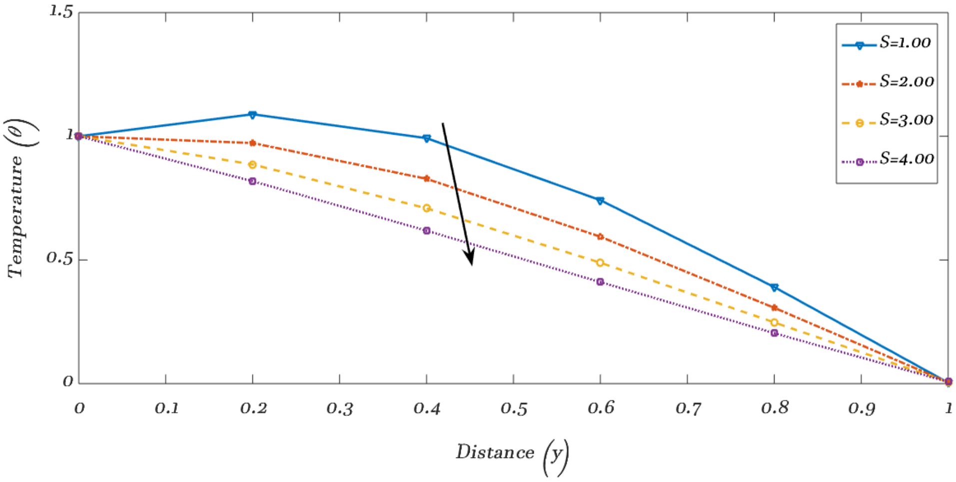

Figure 16: Effect of Suction Parameter S on Temperature Profile

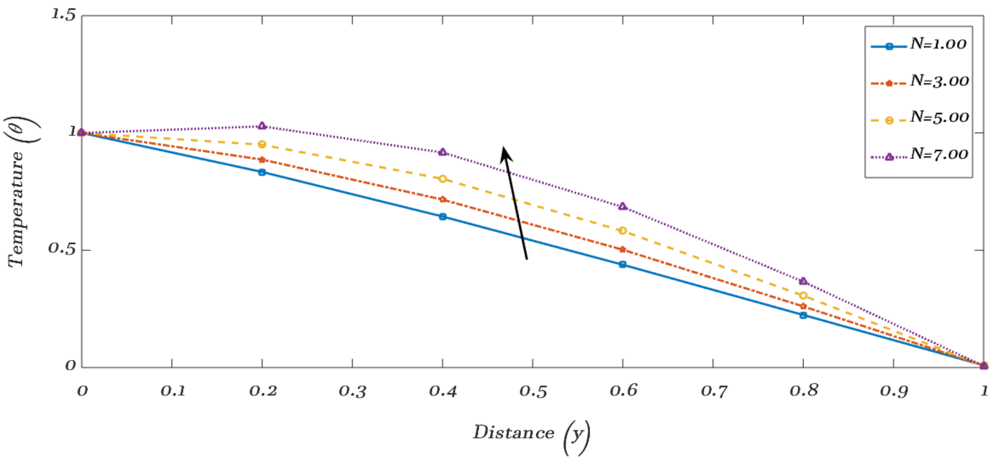

Figure 17: Effect of Radiation Parameter N on Temperature Profile

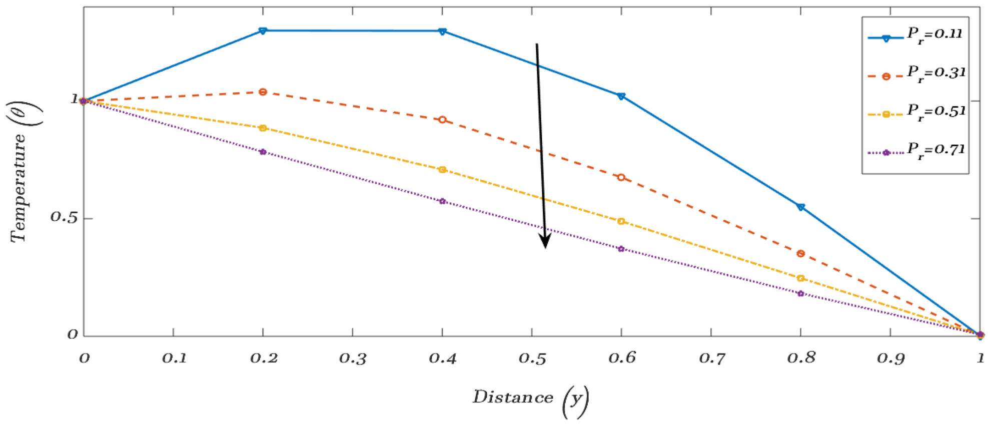

Figure 18: Effect of Prandtl number P_r on Temperature Profile

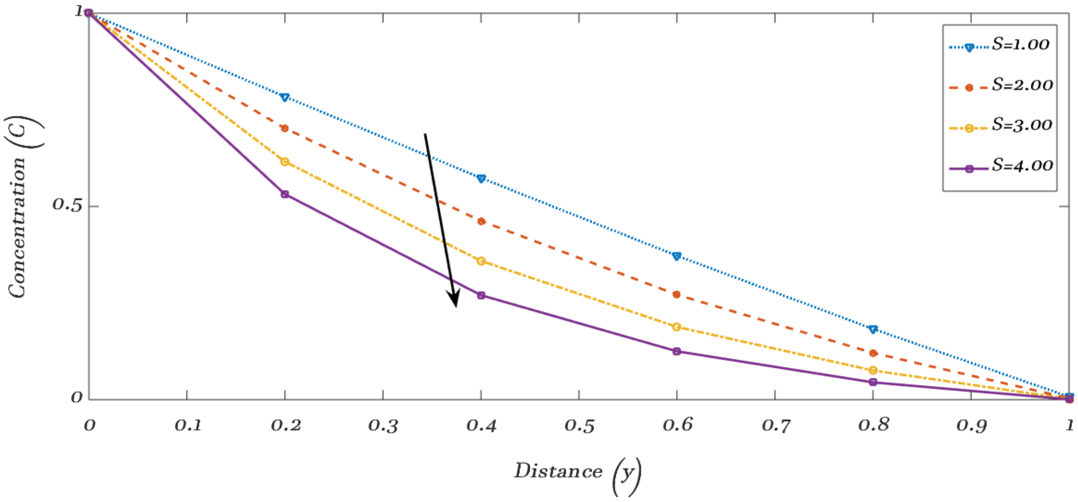

Figure 19: Effect of Suction Parameter S on Concentration Profile

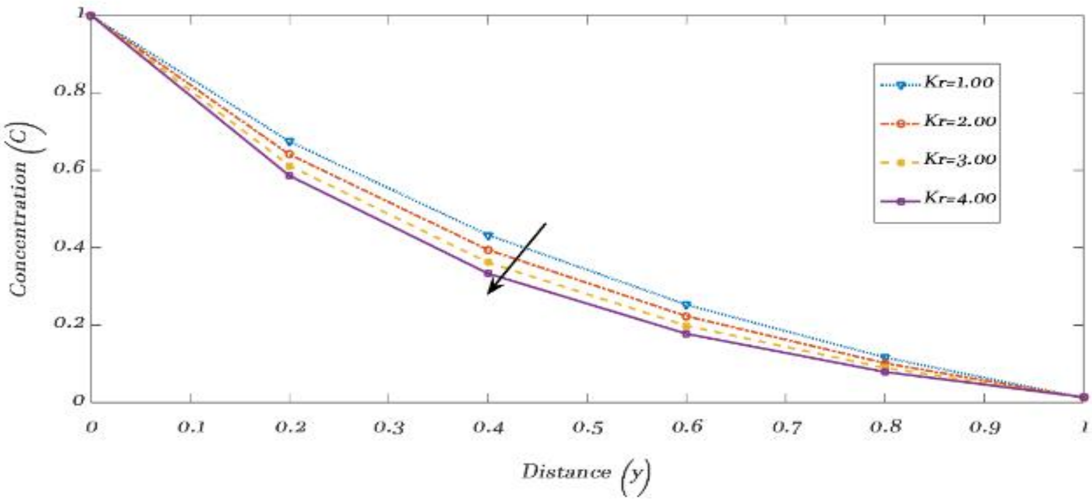

Figure 20: Effect of Chemical Reaction Parameter K_r on Concentration Profile

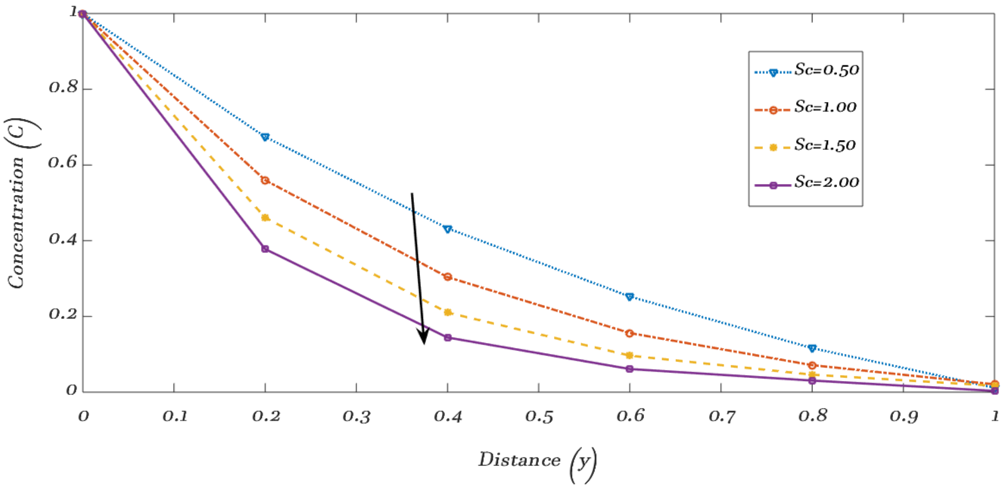

Figure 21: Effect of Schmidt number Sc on Concentration Profile
NOTE**:** Numerical data variation for each parameter is shown on each graph.

Table 1: The computational values for Skin Friction (Cf_0 and Cf_1)

λ	Cf_0	Cf_1	R	Cf_0	Cf_1	Rc	Cf_0	Cf_1	S	Cf_0	Cf_1
0.40	−19.4487	−2.1230	0.00	−19.4199	−2.1110	**0.30**	−17.3956	−2.5184	**1.00**	−19.4199	−2.1110
0.80	−19.5087	−2.1301	0.30	−18.5571	−2.3055	**0.60**	−15.3714	−2.9257	**3.00**	−17.2891	−1.4494
1.20	−19.6315	−2.1987	0.50	−17.9819	−2.4351	**0.90**	−13.3472	−3.3331	**5.00**	−5.9629	−1.0471
1.60	−19.6995	−2.2267	0.70	−17.4067	−2.5647	**1.20**	−11.3230	−3.7404	**7.00**	−3.2147	−0.0648

Source: MATLAB output, 2025

Table 1 shows the computational values for Skin Friction (Cf_0 and Cf_1) for Variable thermal conductivity λ, Temperature buoyancy parameter R, Mass buoyancy parameter R_C and Suction parameter S for both y = 0 and y = 1 respectively.

Table 2: The Computational Values for Nusselt Numbers (Nu_0 and Nu_1)

λ	Nu_0	Nu_1	R	Nu_0	Nu_1	S	Nu_0	Nu_1
0.40	−1.0825	−l0.8454	**0.00**	−1.0866	−0.8387	**1.00**	−1.0866	−0.8387
0.80	−1.0725	−l0.8652	**0.30**	−0.6886	−0.6437	**2.00**	−1.3537	−0.6617
1.20	−1.0697	−0.8853	**0.50**	−0.4232	−0.5137	**3.00**	−1.6517	−0.5129
1.60	−1.0525	−0.8987	**0.70**	−0.1578	−0.3837	**4.00**	−1.9779	−0.3912

Source: MATLAB output, 2025

Table 2 shows the computational values for Nusselt numbers (Nu_0 and Nu_1) respectively for Variable thermal conductivity λ, Temperature buoyancy parameter R and Suction parameter S for both y = 0 and y = 1 respectively.

Table 3: The Computational Values for Sherwood Numbers (Sh_0 and Sh_1)

K_r	Sh_0	Sh_1	S_c	Sh_0	Sh_1	S	Sh_0	Sh_1
1.00	−1.8890	−0.4623	**0.50**	−1.4332	−0.6945	**1.00**	−1.8890	−0.4623
2.00	−2.1612	−0.3867	**1.00**	−1.8890	−0.4623	**2.00**	−2.5958	−0.2490
3.00	−2.4081	−0.3232	**1.50**	−2.3626	−0.3029	**3.00**	−3.4081	−0.1238
4.00	−2.6347	−0.2690	**2.00**	−2.8490	−0.2065	**4.00**	−4.2935	−0.0569

Source: MATLAB output, 2025

Table 3 shows the computational values for Sherwood numbers (Sh_0 and Sh_1) respectively for Chemical reaction parameter K_r , Schmidt number S_C R and Suction parameter S for both y = 0 and y = 1 respectively.
The solutions were simulated for different values of Variable thermal conductivity λ, Temperature buoyancy parameter R, Magnetic parameter M, Mass buoyancy R_C, Suction parameter S, Porosity D_a, Mass Grashof number G_C, Temperature Grashof number G_r, Radiation parameter N, Prandtl number P_r, Chemical reaction K_r, Schmidt number S_c, Pressure gradient Ω , and results were obtained.

Figures 2 to 13 illustrates the velocity profiles for various values. Figure 2 shows velocity U increases as variable thermal conductivity λ increases. Similarly, Figure 3 shows increase in velocity U as R increases. In contrast, Figure 4 shows that increasing the magnetic parameter M leads to a decrease in velocity U. Figure 5 depicts that velocity U increases with increasing R_C, but Figure 6 demonstrates velocity U decreases as the Suction parameter S increases. While increase in Darcy number D_a portrays increase in velocity U in Figure 7. Figure 8 depicts velocity U increases as mass Grashof number G_C increases. Similarly, Figure 9 portrays increasing Radiation parameter N leads to increase in velocity U. Figure 10 observed that velocity U increases with increasing Prandtl number P_r, but decreases with increase chemical reaction parameter K_r as shown in Figure 11. Similarly, Figure 12 shows increase in the Schmidt number S_c also leads to a decrease in velocity U which repeats as pressure gradient Ω increases in Figure 13. The velocity profiles shown in Figures 2 to 13 converge at $y = 0$ and $y = 1$, which correspond to the boundary conditions for the velocity U. The velocity profiles exhibit clear periodic behavior, characteristic of pure oscillations. The temperature profiles have been analyzed and are presented in Figures 14 to 18. Figure 14 reveals that the temperature θ increases with increasing thermal conductivity λ. A similar trend is observed in Figure 15 temperature θ increases with an increase in the temperature buoyancy parameter R. In contrast, Figure 16 shows that temperature θ decreases with increasing suction parameter S, but Figure 17 demonstrates that the temperature θ rises with an increase in the radiation parameter N. While, Figure 18 shows that the temperature θ decreases with increasing Prandtl number P_r. Concentration profile was analyzed in Figures 19 to 21. Figure 19 shows that the concentration C decreases with increasing suction parameter S. A similar decreasing trend is observed in Figure 20 with an increase in the chemical reaction parameter K_r and Likewise, Figure 21 demonstrates that the concentration C decreases with increasing Schmidt number S_c.

Table 1 shows the computational values for Skin Friction (Cf_0 and Cf_1) for Variable thermal conductivity λ, Temperature buoyancy parameter R, Mass buoyancy parameter R_C and Suction parameter S for both y = 0 and y = 1 respectively. It is observed that both coefficients become increasingly negative with rising Variable thermal conductivity λ, indicating that the wall shear stress intensifies as thermal conductivity increases. Although, it is observed that as Temperature buoyancy parameter R increases, Cf_0 becomes progressively less negative. Conversely, Cf_1 shows increasing magnitude with Temperature buoyancy parameter R. While observed that Cf_0 increases steadily (becomes less negative) as Mass buoyancy parameter R_C increases. Conversely, Cf_1 initially decreases (becomes more negative) with increasing Mass buoyancy parameter R_C, But It is evident that as suction increases, both coefficients become less negative. Table 2 shows the computational values for Nusselt numbers (Nu_0 and Nu_1) respectively for Variable thermal conductivity λ, Temperature buoyancy parameter R and Suction parameter S. As Variable thermal conductivity λ increases, both (Nu_0 and Nu_1) become more negative**,** indicating decreased heat transfer at the surface**,** while As Temperature buoyancy parameter R increases, both (Nu_0 and Nu_1) increase (become less negative)**.** Similarly, As Suction S increases, Nu_0 becomes more negative**,** but Nu_1 becomes less negative**.** Table 3 shows the computational values for Sherwood numbers (Sh_0 and Sh_1) respectively for Chemical reaction parameter K_r , Schmidt number S_C and Suction parameter S. The table shows that both (Sh_0 and Sh_1) decrease (become more negative) as the chemical reaction parameter K_r increases. Similarly, an increase in the Schmidt number S_C also causes both (Sh_0 and Sh_1) to become more negative. Although, an increase in the suction parameter S causes Sh_0 to become significantly more negative, indicating stronger mass transfer at the surface due to the removal of solute. In contrast, Sh_1 becomes less negative with increasing S, suggesting reduced mass transfer farther from the wall.

CONCLUSION

This paper studied heat and mass transfer flow through porous medium and investigate the combined effect of variable thermal conductivity and suction. The governing partial differential equations were non-dimensionalized, and solved analytically using the perturbation to study the effects of various dimensionless parameters on the velocity, temperature, and concentration profiles.

The key findings of the study are summarized below:

i. Velocity enhances with increase in Variable Thermal Conductivity λ, temperature and mass buoyancy parameters (R, R_C),Darcy number (D_a), mass Grashof numbers (G_C), radiation parameter (N) and Prandtl number (P_r) but suppresses with magnetic field strength (M), suction parameter and opposing pressure gradient (Ω).

ii. Temperature rises with increase in Variable Thermal Conductivity λ, temperature buoyancy parameters (R) and radiation parameter (N) but decreases with suction parameter (S), and Prandtl number (P_r).

iii. Species concentration reduces with increase in suction parameter (S), chemical reactin rate (K_r) and schimdt number (S_c).

iv. Skin Friction, Nusselt Number, and Sherwood Number: reveal that surface shear stress, heat transfer and mass transfer rates are highly sensitive to thermal conductivity, suction, and chemical reactions.

REFERENCES

Abdullahi, A., & Mahamoudi, Y. (2020). Effect of variable thermal conductivity on heat transfer. *Journal of Applied and Computational Mathematics* 3, (2): 48 – 56 https://doi.org/10.1168/j.acl.20140302.12

Bejan, A. (2013). *Convection heat transfer* (4th ed.). Wiley. [Chapter 2: Scaling and Non-dimensional Parameters]

Bird, R. V., Stewart W. E., & Lightfoot E. N. (2002). *Transport phenomena* (2nd Ed.) John Wiley & Sons.

Cengel, Y. A., & Boles, M. A. (2020). *Thermodynamics: An integrated approach (8TH Ed.)*. McGraw-Hill Education. ISBN 978-126043333

Dekker, Mercel (2000). "*Handbook of porous media*". New York. Basel, Switzerland

Incropera, F. P., & DeWitt D. P. (2018). *Fundamentals of heat and mass transfer*. John Willey & Sons

Ingham, D. B., & Pop, I. (2017). *Transport phenomena in porous media*. Elsevier.

Kaita, I. H., Zayyanu, S. Y., Mas'ud, L., Hamisu, A., Abdullahi, U. & Auwal, D. M. (2024). Heat and mass transfer flow in a channel filled with porous medium in the presence of variable thermal conductivity. *FUDMA Journal of Sciences* (FJS), https://doi.org/10.33003/fjs-2024-0802-2236.

Kaviany, M. (2012). *Principles of heat transfer in porous media*. Springer-Verlag.

Kuznetsov, A. V., & Nield, D. A. (2013). Heat transfer in a channel filled with a Porous Medium: Effects of variable thermal conductivity. International. *Journal of Heat and Mass Transfer*, 66, 772-781.

Mahmoudi, Y., Karimi, N., & Mazaheri, K. (2017). Mass transfer in a channel filled with a porous medium: effects of variable thermal conductivity. Transport in Porous Media, 116(2), 257-273.

Nasrin, R. & Alim, M. A. (2009). MHD Free convection flow along a vertical flat plate with thermal conductivity and viscosity depending on temperature. *Journal of Naval Architecture and Marine Engineering,* 6:72-83. https://www.researchgate.net/publication/285136857

Nield, D. A. & Bejan, A. (2017). *Convection in Porous Media, Fifth Edition. Springer*, New York. https://link.springer.com/book/10.1007/978-3-319-49562-0

Nayfeh, A. H. (2000). *Perturbation methods*. John Wiley & Sons.

Rashidi, S. & Esfahani, J. A. (2019). Variable thermal conductivity on heat transfer in porous channel. *Journal of Porous Media*, 22(3), 257-271.

Rashidi, S. & Esfahani, J. A. (2020). Suction effect on heat transfer in porous media. *Journal of Thermal Analysis,* 23(5), 457-471

Singh, P. & Kumar, V. (2020). Variable thermal conductivity and suction effect on heat transfer in porous channel. *Journal of Thermal Science and Engineering Applications*, 12(2), 021001.

Singh, P., Kumar, V., & Gupta, M. (2019). Numerical study of heat transfer in a channel filled with a porous medium: Effects of suction. *Journal of Porous Media,* 22(10), 931-944.

Singh, R., & Kasana, H.S. (2019). Thermal conductivity of porous media: A review. *Journal of porous media* 22(1), 1-15.